Optics Letters

Reconfigurable opto-thermal graded-index waveguiding in bulk chalcogenide glasses

Soroush Shabahang,[1] Nicholas S. Nye,[1] Christos Markos,[1,2] Demetrios N. Christodoulides,[1] and Ayman F. Abouraddy[1,*]

[1]CREOL, The College of Optics & Photonics, University of Central Florida, Orlando, Florida 32816, USA
[2]DTU Fotonik, Department of Photonics Engineering, Technical University of Denmark, DK-2800 Kgs. Lyngby, Denmark
*Corresponding author: raddy@creol.ucf.edu

Received 22 March 2017; revised 15 April 2017; accepted 16 April 2017; posted 17 April 2017 (Doc. ID 291220); published 5 May 2017

In the absence of suitable deposition processes, the fabrication of graded-index chalcogenide waveguides or fibers remains an outstanding challenge. Here, by exploiting the strong thermo-optic effect present in chalcogenide glasses, we experimentally demonstrate non-permanent optically-induced waveguides in bulk As_2Se_3 rods using a 1.55 μm wavelength laser. This single-step process can be used not only to self-trap the writing beam, but also to guide another optical beam at a different wavelength in the opto-thermally inscribed waveguide channel. These results could pave the way towards harnessing nonlinear effects in graded-index chalcogenide guided settings.

OCIS codes: (160.2750) Glass and other amorphous materials; (160.6840) Thermo-optical materials; (260.5950) Self-focusing; (350.5340) Photothermal effects; (230.7380) Waveguides, channeled.

https://doi.org/10.1364/OL.42.001919

Chalcogenide glasses (ChGs) are characterized by a broad mid-infrared (mid-IR) transparency window, high refractive indices, and large third-order nonlinearities [1,2]. Such exceptional attributes make them ideal candidates for mid-IR applications [3]. For example, ChGs have been exploited in producing mid-IR fibers [4] since silica glass, the dominant optical material for fiber technologies, becomes opaque beyond a wavelength of ~2.2 μm. Over the last decade, developments in fabrication processes have led to rapid progress in the field of ChG photonics [5]. Novel structures such as photonic crystal fibers [6,7], multimaterial fibers [8,9], and robust ChG multimaterial step-index fibers [10,11] have led to applications in all-optical signal processing [12,13] and supercontinuum generation in high-NA ChG fibers [14–18]. Furthermore, because ChGs are composed of a unique class of amorphous semiconductors, multimaterial fibers incorporating ChGs can be used to construct optical [19,20] and thermal [21] fiber detectors.

Motivated by such advances, emphasis has been given to the development of high-performance guiding structures in ChGs. In this respect, a number of approaches have been devised, including chemical vapor deposition [22], photodoping [23], thermal evaporation [24], dry-etching [25,26], pulsed laser deposition [27,28] and exploiting the photosensitivity of ChGs [29–31]. Progress has also been made in the fabrication of waveguide channels on non-planar substrates and in three-dimensional ChG configurations via femtosecond direct laser writing [32–35], thermal nano-imprinting [36,37], and direct holographic writing [38], to mention a few. Nevertheless, it should be emphasized that, in almost all the previous approaches, the photo-structural changes imposed on the ChGs are non-reversible and are better suited for ridge-like waveguide structures. Despite this progress, the arsenal of ChG photonics still lacks graded-index waveguides, a class of structures that recently have generated considerable interest [39,40]. Although the fabrication of graded-index fibers has a long history, a comparable technology for ChGs has been lacking.

In this Letter, we explore an alternative avenue for establishing *non-permanent graded-index waveguides* in the bulk ChG As_2Se_3 based on the thermo-optic effect. Furthermore, we observe here for the first time, to the best of our knowledge, nonlocal spatial soliton formation [41–49] in bulk ChGs. Although similar effects have been investigated in lead-silicate glasses [43–49] and active fiber systems [50], the high thermo-optic coefficient of ChGs, along with their low thermal conductivity, makes them particularly suitable candidates for dynamic laser inscription of waveguides. In our experiments, a Gaussian beam traverses a ChG rod and induces a transverse temperature gradient that locally modifies the refractive index distribution. At a sufficiently high power (~250 mW), this index modulation provides the necessary contrast to self-trap the writing beam and/or guide a second co- or counter-propagating probe beam at a different wavelength (Fig. 1). By controlling the intensity and shape of the writing beam, one can judiciously engineer the refractive index profile of the opto-thermally-induced waveguide. Our experimental results are in excellent agreement with coupled-mode equations that model the combined opto-thermal dynamics of the system.

We begin our theoretical analysis by considering the spatio-temporal interplay between optical-wave-propagation effects and heat diffusion to estimate the power required for opto-thermal waveguide inscription. In the case of a self-trapped writing beam, the combined opto-thermal dynamics in a material having an optical loss coefficient α and refractive

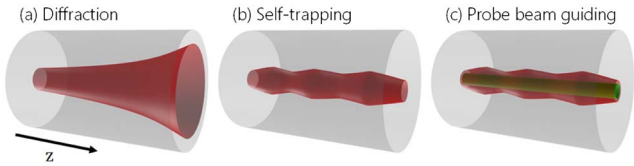

Fig. 1. Illustration of the optical dynamics governing the propagation in a ChG rod at different power levels P of the writing beam (red). (a) At low P, the writing beam undergoes diffraction. (b) When P exceeds a critical value (~250 mW), it is self-trapped. (c) Once P exceeds the critical value in (b), it can guide a co- or counter-propagating probe beam at a different wavelength (green) via the opto-thermally-induced graded-index waveguide.

index n_o at the pump wavelength $\lambda_o = 1.55$ μm, density ρ, specific heat capacity c_ρ, thermal conductivity κ, and thermo-optic coefficient $\gamma = dn/dT$ are described by the coupled equations:

$$i\frac{\partial \mathcal{E}}{\partial Z} + \nabla_\perp^2 \mathcal{E} + i\frac{\tilde{\alpha}}{2}\mathcal{E} + \Theta\mathcal{E} = 0, \quad \frac{\partial \Theta}{\partial \tau} = \nabla_\perp^2 \Theta + |\mathcal{E}|^2. \quad \textbf{(1)}$$

In the above equations, $\mathcal{E} = E/E_o$ is the normalized envelope of the optical field, and $\Theta = \Delta T/T_o$ is the normalized temperature difference with respect to the ambient environment, where

$$E_o = \sqrt{\frac{\kappa \eta_o}{\alpha \gamma n_o^2 k_o^2 w_o^4}}, \quad T_o = \frac{1}{2k_o^2 n_o \gamma w_o^2}. \quad \textbf{(2)}$$

In addition, η_o, $k_o = 2\pi/\lambda_o$, and λ_o are the free-space characteristic impedance, wavenumber, and wavelength, respectively. The transverse coordinates involved in the Laplacian operator $\nabla_\perp^2 = \partial^2/\partial X^2 + \partial^2/\partial Y^2$ are dimensionless, $X = x/w_o$, and $Y = y/w_o$, with w_o representing an arbitrary transverse scale; the axial propagation distance $Z = z/z_o$, time $\tau = t/t_o$, and loss coefficient $\tilde{\alpha} = \alpha z_o$ are appropriately normalized, with $z_o = 2k_o n_o w_o^2$ and $t_o = w_o^2 \rho c_\rho/\kappa$. The ChG used in our experiment is characterized by $\rho = 4630$ kg/m^3, $c_\rho = 360$ J/(K · kg), $\alpha = 3.4$ m^{-1}, $\kappa = 0.15$ W/(K · m), $n_o = 2.85$ at $\lambda_o = 1.55$ μm, and $\gamma = +6.5 \cdot 10^{-5}$ K^{-1}.

Simulations under steady-state conditions indicate that the critical power needed to establish a nonlocal spatial soliton [41–49] by balancing diffraction with thermal self-focusing effects is ~250 mW for this system (Fig. 2). At low powers, diffractive spreading leads to an increase in the beam's size at the exit and drop in power axially. At higher powers, the local index at the beam center is elevated via the thermo-optic effect, leading to self-guidance. This occurs at ~250 mW, whereupon the opto-thermally-induced refractive index change on axis is $\Delta n \approx 10^{-4}$. A focus emerges at 9 cm and the opto-thermally-induced index profile corresponds to a graded-index waveguide. The thermal nonlinearity becomes more prominent with further increase in power, resulting in the emergence of additional foci along the beam path within the As_2Se_3 rod [Figs. 2(c) and 2(d)].

This process is to some extent analogous to that of spatial soliton formation due to the optical Kerr effect. In the latter case, self-focusing occurs due to an instantaneous intensity-dependent refractive index change while, in opto-thermal media. the index changes take place in a more cumulative fashion, leading in that manner to a non-local spatial soliton beam.

The experimental setup used to demonstrate the opto-thermal waveguiding effect is illustrated in Fig. 3. The writing beam inscribing the graded-index waveguides is a 1.55 μm

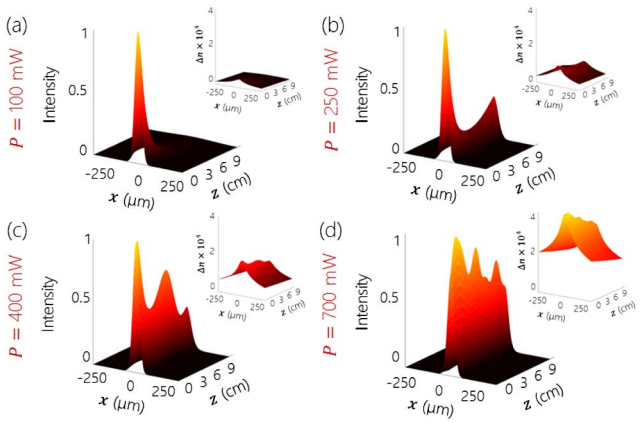

Fig. 2. Beam propagation results describing the evolution of the 1.55 μm wavelength writing beam for different powers P under steady-state conditions along a bulk As_2Se_3 rod: (a) $P = 100$ mW, (b) 250 mW, (c) 400 mW, and (d) 700 mW. The insets show the corresponding opto-thermally-induced refractive index distribution.

wavelength continuous-wave (CW) laser delivering up to 700 mW of power. Experiments for self-trapping of the writing beam were carried out in a 9.3 cm long, 1 cm diameter As_2Se_3 rod [Fig. 3(a)]. The writing laser is focused to a 50 μm diameter spot at the entrance to the ChG rod, whose length is an order of magnitude larger than the beam Rayleigh range inside the material. At low power levels, the beam diffracts and emerges with a larger diameter. The beam then gradually self-focuses with increasing power. A comparison of the experimentally captured output beam profiles and the results of nonlinear beam propagation calculations [Eqs. (1) and (2)] at different input powers reveal excellent *quantitative* agreement (Fig. 4).

At a writing beam power of 400 mW, the beam refocuses closer to the input facet of this rod, as indicated by both our

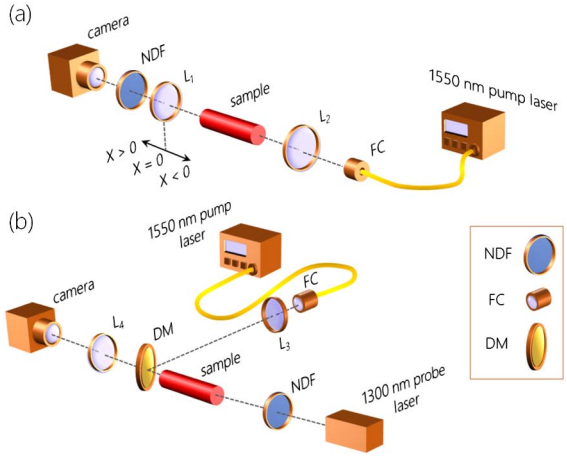

Fig. 3. (a) Experimental setup for the opto-thermal inscription of a graded-index waveguide by a 1.55 μm wavelength writing beam in a 9.3 cm long As_2Se_3 rod, and (b) for guiding of a second counter-propagating low-power 1.3 μm wavelength probe beam within a waveguide opto-thermally induced by the 1.55 μm writing beam in a 2.5 cm long As_2Se_3 rod. NDF, neutral density filter; FC, fiber collimator; DM, dichroic mirror. NDFs are used to reduce the optical power reaching the camera. Lenses L_1, L_2, L_3, and L_4 have focal lengths of 10, 30, 30, and 7.5 cm, respectively.

experimental and simulation results in Figs. 2(c) and 4(b). For even higher pump powers, the writing beam self-focuses faster, and intensity modulations (soliton breathing) become even more pronounced [Figs. 2(d) and 4(c)]. In this regime, the maximum thermo-optic refractive index change is $\Delta n \approx 4 \times 10^{-4}$.

Experiments for guiding a counter-propagating low-power 1.3 μm wavelength probe beam were performed in a shorter 2.5 cm long As_2Se_3 rod [Fig. 3(b)] in which the waveguide channel was opto-thermally induced by the 1.55 μm CW writing beam. The thermo-optic refractive index contrast was interferometrically estimated by monitoring the optical ring sidelobes produced in the presence of this graded-index waveguide and verified by our simulation results. In this case, the spatial evolution of the probe beam in a material having a loss coefficient α_p and refractive index n_p at the probe wavelength ($\lambda_p = 1.3$ μm) is governed by the following paraxial wave dynamics:

$$i\frac{\partial \mathcal{E}_p}{\partial Z} + \nabla_\perp^2 \mathcal{E}_p + i\frac{\tilde{\alpha}_p}{2}\mathcal{E}_p + V\mathcal{E}_p = 0. \quad \textbf{(3)}$$

In the above equation, $\mathcal{E}_p$ and $V = 2k_p^2 n_p \Delta n w_o^2$ are the normalized optical field envelope and optical potential, respectively, where $k_p = 2\pi/\lambda_p$ is the free-space wavenumber and $\Delta n = \gamma \Delta T$ is the refractive index contrast opto-thermally induced by the writing beam, as shown by the insets of Fig. 2. In addition, $\tilde{\alpha}_p = \alpha z_p$ is the normalized attenuation coefficient, with $z_p = 2k_p n_p w_o^2$. The As_2Se_3 sample used in the experimental setup is characterized by $\alpha_p \approx \alpha = 3.4\,\mathrm{m}^{-1}$ and $n_p \approx_o = 2.85$ at $\lambda_p = 1.3$ μm.

A different experimental arrangement [Fig. 3(b)] is employed in which a low-power ~1 mW, 1.3 μm wavelength counter-propagating probe beam is guided through the inscribed waveguide thermally induced by the above-described 1.55 μm, ~50 μm diameter writing beam. In this setup, the writing beam is collimated and then focused onto a 2.5 cm long ChG rod using a fiber collimator and a lens having a 30 cm focal length. A dichroic mirror orientated at 45° with respect to the beam is inserted in the beam path. The dichroic mirror reflects ≥95% at 1.55 μm and transmits more than 95% at 1.3 μm. While the input probe beam covers the entire facet of the As_2Se_3 rod, only a fraction of it gets eventually trapped in the waveguide channel, induced by the 1.55 μm pump.

We present our experimental results and simulations of this configuration in Fig. 5. Once self-trapping is established in the pump (~250 mW), the width of the 1.3 μm probe beam stabilizes to ~30 μm at the output. In essence, one can effectively guide a probe beam (of different wavelengths) in the same photo-thermally-induced graded-index waveguide.

As the power of the pump beam increases, the guiding becomes even more prominent and, when it reaches 700 mW, an additional ring appears around the central bright spot of the probe [Fig. 5(c)]. This effect, a variant of the Poisson spot, results from interference and can be used to experimentally estimate the index contrast of the induced waveguide. More specifically, by calculating the distance between the central bright spot and the sidelobe ring, in conjunction with the free-space distance traveled by the probe beam until it reaches the ChG sample, we estimated a maximum index change of $\Delta n \approx 4 \times 10^{-4}$ ($\Delta T \approx 6$ K), which was independently verified by our simulations. In order to further explain the observed ring structure in the probe beam, we have carried out additional simulations (Fig. 6) for different pump power levels. When the probe beam diameter is 50 μm, the ring sidelobe disappears altogether, since the fundamental mode of the waveguide channel is now mainly excited, in contrast to the case presented in Fig. 5, where interference takes place between a number of modes. Moreover, above 250 mW, the probe is always effectively captured in the induced opto-thermal waveguide.

In conclusion, we have experimentally demonstrated the opto-thermal inscription of non-permanent optical waveguides

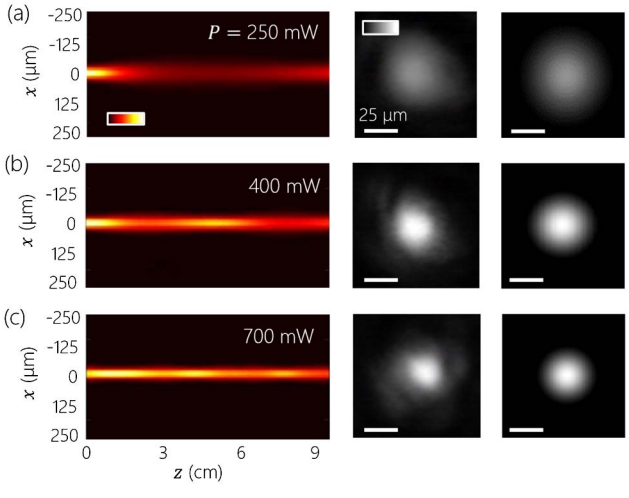

Fig. 4. Experimental and simulation results for the setup of Fig. 3(a) for different powers of the writing 1.55 μm beam under steady-state conditions: (a) $P = 250$ mW, (b) 400 mW, and (c) 700 mW. The left column shows the evolution of the 1.55 μm writing beam within the 9.3 cm long As_2Se_3 rod, as obtained numerically. The center and right columns depict experimental results and theoretical predictions, respectively, of the beam intensity profile at the exit of the rod. All of the scale bars are 25 μm.

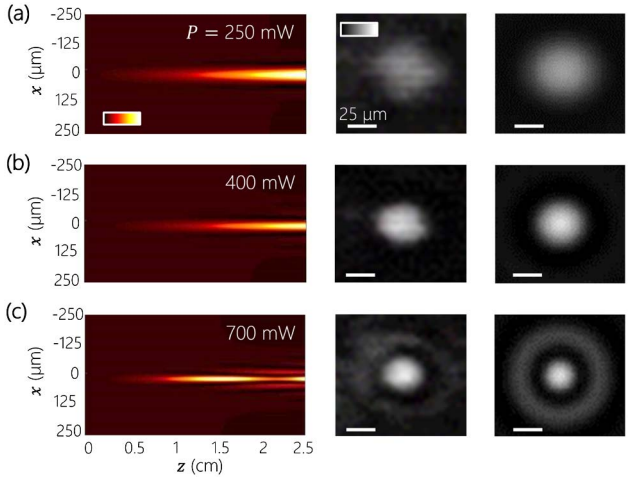

Fig. 5. Measurements and simulations for the opto-thermal guidance—via a 1.55 μm writing beam—of a counter-propagating 1.3 μm probe beam [Fig. 3(b)]. We plot the results for different powers of the writing beam: (a) $P = 250$ mW, (b) 400 mW, and (c) 700 mW. The left column shows the simulated evolution of the intensity of the 1.3 μm probe beam along a 2.5 cm long As_2Se_3 rod. The center and right columns depict experimental and theoretical results, respectively, for the output beam intensity profile at the exit of the rod. In all cases, the probe beam at the input is considered to be much broader than the pump. All the scale bars are 25 μm.

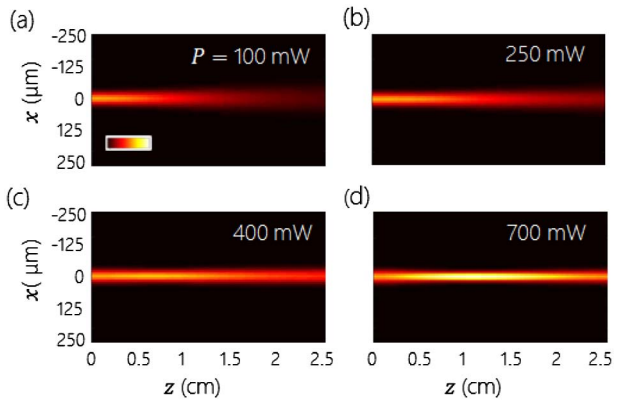

Fig. 6. Beam propagation results for the setup of Fig. 3(b) describing the evolution of a 50 μm diameter, 1.3 μm probe beam for different pump powers: (a) $P = 100$ mW, (b) 250 mW, (c) 400 mW, and (d) 700 mW.

in bulk As_2Se_3 ChG rods using a conventional low-cost 1.55 μm writing laser beam. This method exploits the high thermo-optic coefficient of ChGs, as well as their low thermal conductivity. At sufficiently high power levels, the pump was found to self-trap itself by establishing a graded-index waveguide that can guide a probe beam at a different wavelength. Our method could pave the way towards harnessing nonlinear effects in graded-index ChG waveguides.

Funding. National Science Foundation (NSF) (1500292, 1420620); Office of Naval Research (ONR) (N00014-13-1-0649); Qatar National Research Fund (QNRF) (9-020-1-006); Alexander S. Onassis Public Benefit Foundation; Foundation for Education and European Culture (IPEP); FTP (4184-00359B); ShapeOCT (4107-00011A).

REFERENCES

1. M. Asobe, Opt. Fiber Technol. **3**, 142 (1997).
2. A. Zakery and S. Elliott, J. Non-Crystal. Solids **330**, 1 (2003).
3. J. Sanghera and I. Aggarwal, J. Non-Crystal Solids **256–257**, 6 (1999).
4. G. Tao, H. Ebendorff-Heidepriem, A. M. Stolyarov, S. Danto, J. V. Badding, Y. Fink, J. Ballato, and A. F. Abouraddy, Adv. Opt. Photon. **7**, 379 (2015).
5. B. J. Eggleton, B. Luther-Davies, and K. Richardson, Nat. Photonics **5**, 141 (2011).
6. T. M. Monro, Y. D. West, D. W. Hewak, N. Broderick, and D. Richardson, Electron. Lett. **36**, 1998 (2000).
7. B. Temelkuran, S. D. Hart, G. Benoit, J. D. Joannopoulos, and Y. Fink, Nature **420**, 650 (2002).
8. A. F. Abouraddy, M. Bayindir, G. Benoit, S. D. Hart, K. Kuriki, N. Orf, O. Shapira, F. Sorin, B. Temelkuran, and Y. Fink, Nat. Mater. **6**, 336 (2007).
9. G. Tao, A. M. Stolyarov, and A. F. Abouraddy, Int. J. Appl. Glass Sci. **3**, 349 (2012).
10. G. Tao, S. Shabahang, E.-H. Banaei, J. J. Kaufman, and A. F. Abouraddy, Opt. Lett. **37**, 2751 (2012).
11. G. Tao, S. Shabahang, H. Ren, F. Khalilzadeh-Rezaie, R. E. Peale, Z. Yang, X. Wang, and A. F. Abouraddy, Opt. Lett. **39**, 4009 (2014).
12. S. Madden, D.-Y. Choi, D. Bulla, A. V. Rode, B. Luther-Davies, V. G. Ta'eed, M. Pelusi, and B. J. Eggleton, Opt. Express **15**, 14414 (2007).
13. M. R. Lamont, B. Luther-Davies, D.-Y. Choi, S. Madden, X. Gai, and B. J. Eggleton, Opt. Express **16**, 20374 (2008).
14. D.-I. Yeom, E. C. Mägi, M. R. Lamont, M. A. Roelens, L. Fu, and B. J. Eggleton, Opt. Lett. **33**, 660 (2008).
15. S. Shabahang, M. P. Marquez, G. Tao, M. U. Piracha, D. Nguyen, P. J. Delfyett, and A. F. Abouraddy, Opt. Lett. **37**, 4639 (2012).
16. S. Shabahang, G. Tao, M. P. Marquez, H. Hu, T. R. Ensley, P. J. Delfyett, and A. F. Abouraddy, J. Opt. Soc. Am. B **31**, 450 (2014).
17. C. R. Petersen, U. Møller, I. Kubat, B. Zhou, S. Dupont, J. Ramsay, T. Benson, S. Sujecki, N. Abdel-Moneim, Z. Tang, D. Furniss, A. Seddon, and O. Bang, Nat. Photonics **8**, 830 (2014).
18. J. Hu, C. R. Menyuk, L. B. Shaw, J. S. Sanghera, and I. D. Aggarwal, Opt. Express **18**, 6722 (2010).
19. M. Bayindir, F. Sorin, A. F. Abouraddy, J. Viens, S. D. Hart, J. D. Joannopoulos, and Y. Fink, Nature **431**, 826 (2004).
20. A. F. Abouraddy, O. Shapira, M. Bayindir, J. Arnold, F. Sorin, D. S. Hinczewski, J. D. Joannopoulos, and Y. Fink, Nat. Mater. **5**, 532 (2006).
21. M. Bayindir, J. D. J. A. F. Abouraddy, J. Arnold, and Y. Fink, Adv. Mater. **18**, 845 (2006).
22. C. Huang, D. Hewak, and J. Badding, Opt. Express **12**, 2501 (2004).
23. R. G. DeCorby, N. Ponnampalam, M. M. Pai, H. T. Nguyen, P. K. Dwivedi, T. J. Clement, C. J. Haugen, J. N. McMullin, and S. O. Kasap, IEEE J. Sel. Top. Quantum Electron. **11**, 539 (2005).
24. J.-F. Viens, C. Meneghini, A. Villeneuve, T. V. Galstian, E. J. Knystautas, M. Duguay, K. Richardson, and T. Cardinal, J. Lightwave Technol. **17**, 1184 (1999).
25. Y. Ruan, W. Li, R. Jarvis, N. Madsen, A. Rode, and B. Luther-Davies, Opt. Express **12**, 5140 (2004).
26. J. Hu, V. Tarasov, A. Agarwal, L. Kimerling, N. Carlie, L. Petit, and K. Richardson, Opt. Express **15**, 2307 (2007).
27. K. Youden, T. Grevatt, R. Eason, H. Rutt, R. Deol, and G. Wylangowski, Appl. Phys. Lett. **63**, 1601 (1993).
28. A. Zakery, Y. Ruan, A. V. Rode, M. Samoc, and B. Luther-Davies, J. Opt. Soc. Am. B **20**, 1844 (2003).
29. K. Shimakawa, A. Kolobov, and S. Elliott, Adv. Phys. **44**, 475 (1995).
30. C. Meneghini and A. Villeneuve, J. Opt. Soc. B **15**, 2946 (1998).
31. G. Yang, H. Jain, A. Ganjoo, D. Zhao, Y. Xu, H. Zeng, and G. Chen, Opt. Express **16**, 10565 (2008).
32. O. Efimov, L. Glebov, K. Richardson, E. Van Stryland, T. Cardinal, S. Park, M. Couzi, and J. Bruneel, Opt. Mater. **17**, 379 (2001).
33. A. Zoubir, M. Richardson, C. Rivero, A. Schulte, C. Lopez, K. Richardson, N. Hô, and R. Vallée, Opt. Lett. **29**, 748 (2004).
34. A. Ródenas, G. Martin, B. Arezki, N. Psaila, G. Jose, A. Jha, L. Labadie, P. Kern, A. Kar, and R. Thomson, Opt. Lett. **37**, 392 (2012).
35. S. Wong, M. Deubel, F. Pérez-Willard, S. John, G. A. Ozin, M. Wegener, and G. von Freymann, Adv. Mater. **18**, 265 (2006).
36. T. Han, S. Madden, D. Bulla, and B. Luther-Davies, Opt. Express **18**, 19286 (2010).
37. Y. Zou, D. Zhang, H. Lin, L. Li, L. Moreel, J. Zhou, Q. Du, O. Ogbuu, S. Danto, J. D. Musgraves, K. Richardson, K. D. Dobson, R. Birkmire, and J. Hu, Adv. Opt. Mater. **2**, 478 (2014).
38. A. Feigel, Z. Kotler, B. Sfez, A. Arsh, M. Klebanov, and V. Lyubin, Appl. Phys. Lett. **77**, 3221 (2000).
39. J. Carpenter, B. J. Eggleton, and J. Schröder, Nat. Photonics **9**, 751 (2015).
40. L. G. Wright, Z. Liu, D. A. Nolan, M.-J. Li, D. N. Christodoulides, and F. W. Wise, Nat. Photonics **10**, 771 (2016).
41. W. Królikowski and O. Bang, Phys. Rev. E **63**, 016610 (2000).
42. D. Briedis, D. E. Petersen, D. Edmundson, W. Krolikowski, and O. Bang, Opt. Express **13**, 435 (2005).
43. F. Dabby and J. Whinnery, Appl. Phys. Lett. **13**, 284 (1968).
44. A. S. Desyatnikov, D. Neshev, E. A. Ostrovskaya, Y. S. Kivshar, G. McCarthy, W. Krolikowski, and B. Luther-Davies, J. Opt. Soc. Am. B **19**, 586 (2002).
45. C. Rotschild, O. Cohen, O. Manela, M. Segev, and T. Carmon, Phys. Rev. Lett. **95**, 213904 (2005).
46. C. Rotschild, B. Alfassi, O. Cohen, and M. Segev, Nat. Phys. **2**, 769 (2006).
47. B. Alfassi, C. Rotschild, O. Manela, M. Segev, and D. N. Christodoulides, Phys. Rev. Lett. **98**, 213901 (2007).
48. B. Alfassi, C. Rotschild, and M. Segev, Phys. Rev. A **80**, 041808 (2009).
49. R. Bekenstein, R. Schley, M. Mutzafi, C. Rotschild, and M. Segev, Nat. Phys. **11**, 872 (2015).
50. F. Jansen, F. Stutzki, H.-J. Otto, T. Eidam, A. Liem, C. Jauregui, J. Limpert, and A. Tünnermann, Opt. Express **20**, 3997 (2012).